Detection of Bilayer Packing Stress and Its Release in Lamellar-Cubic Phase Transition by Time-Resolved Fluorescence Anisotropy

Minoru Nakano,* Tomoari Kamo, Atsuhiko Sugita, and Tetsurou Handa

Graduate School of Pharmaceutical Sciences, Kyoto University, Sakyo-ku, Kyoto 606-8501, Japan

Received: August 24, 2004; In Final Form: November 30, 2004

An introduction of nonlamellar-forming lipids into planar bilayers generates packing stress, which is important for the biological functions of plasma membranes and is a driving force for the lamellar-nonlamellar phase transition. We have investigated the phase behavior of a binary system consisting of egg yolk phosphatidylcholine and monoolein (MO) and the changes in the local orientation order of lipids in a lamellar-bicontinuous cubic phase transition. Small-angle X-ray scattering has revealed that the lamellar-bicontinuous cubic phase transition occurs at an MO molar fraction (X_{MO}) between 0.6 and 0.7. These phases were dispersed to form liposomes and cubosomes to monitor the anisotropy of the incorporated fluorescence probe, in which Pluronic F127, used as a dispersion stabilizer of the cubic phase, has been proven not to alter the cubic structure and the location of the probes. Time-resolved fluorescence anisotropy measurements on these dispersions have revealed that the order parameter of the probe in the lamellar phase increases with increasing X_{MO}, and that it decreases during the transition to the cubic phase. This observation suggests that packing stress generated by the addition of the nonlamellar-forming lipid is released by the phase transition.

Introduction

Plasma membranes generally consist of planar lipid bilayers. However, it is well-known that "nonlamellar-forming lipids", which form a nonlamellar structure such as an inverted hexagonal (H_{II}) or a bicontinuous cubic phase by themselves, have an important role in dynamic functions of membranes such as fusion and regulation of lipid composition.[1−4]

When lipids possessing a negative spontaneous curvature, such as phosphatidylethanolamine or diacylglyceride, are forced to form the planar bilayer structure, the membrane acquires packing stress,[5] which comes from a deviation of the membrane mean curvature from the spontaneous curvature of the lipids. It is considered that packing stress increases until the membranes reach a lamellar-nonlamellar phase transition and that stress is released by the transition, when the membrane acquires the negative curvature. Packing stress has been assumed to control the function and structure of membrane proteins.[6−8] It also affects enzymatic activities of soluble proteins functioning at the membrane surface such as phospholipase A_2 [9] and phospholipase C[10] due to the change in susceptivity of the substrates. It has been also demonstrated that the activity of CTP: phosphocholine cytidylyltransferase, a rate-limiting enzyme in phosphatidylcholine biosynthesis, is modulated by membrane curvature elastic stress.[11]

Despite their importance in biological relevance, there are few reports that have investigated the physicochemical properties of the membranes in the presence of the nonbilayer structures and packing stress. One of the reasons may be that the nonlamellar structures cannot be dispersed by themselves in the aqueous phase to form stable and small particles. For the lamellar phase, on the other hand, lipid dynamics and peptide conformation in this phase can be investigated using its dispersion, liposomes, by means of fluorescence or circular dichroism. These analytical techniques can be applied only to a system with low turbidity. Cheng and co-workers have extensively investigated to observe packing defects in the lamellar-inverted hexagonal phase transition by means of time-resolved fluorescence depolarization of diphenylhexatriene (DPH) analogues[12−16] and intramolecular excimer formation of pyrene-labeled lipids.[17−19] Although they have used liposomes for these experiments, close attention has been paid to the aggregation of liposomes after phase transition.[17] In addition, the lamellar-inverted hexagonal phase transition in the system they have used occurs at rather broad composition region, so that the release of packing stress has not been clearly observed. Although NMR may probe the packing constraints in lipid bilayers,[20] the order parameter determination of acyl chains of lipids by NMR[21] cannot be applied to the cubic phases because it provides only isotropic signals; that is, the time scale of NMR (10^{-5} s) is extremely long compared with the translational diffusion of lipids.

Previously, we have successfully prepared the dispersion of the bicontinuous cubic and H_{II} phases, cubosome and hexosome, by high-pressure emulsification using Pluronic F127 as an emulsifier.[22−24] These nanoparticles can be a great tool for the investigation of the nonlamellar structures, because ^{13}C NMR studies have demonstrated that molecular interactions and dynamic properties of cubosome and hexosome are closely related to the nondispersed phases.[25] Fluorescence anisotropy measurement can be applied only to the dispersions but not to the nondispersed systems as described in Discussion section. In this study, the fluorescence measurements are applied to this cubosome system in addition to liposome, to observe packing stress and its release in the lamellar-nonlamellar phase transition. Egg yolk phosphatidylcholine and monoolein are used as lamellar- and nonlamellar-forming lipids since they form lamellar and bicontinuous cubic phases at fully hydrated state, respectively.

Materials and Methods

Materials. Monoolein (1-Monooleoyl glycerol, MO, purity > 99%) was supplied from NOF Corp. (Tokyo). Egg

* Corresponding author. Tel.: +81-75-753-4565. Fax: +81-75-753-4601. E-mail: mnakano@pharm.kyoto-u.ac.jp.

10.1021/jp046181z CCC: $30.25
Published on Web 02/19/2005

yolk phosphatidylcholine (EPC, purity > 99%) was provided by Asahi Kasei Co. (Tokyo). 1-Palmitoyl-2-oleoyl-sn-glycero-3-phosphocholine (POPC) was purchased from Sigma Chemical Co. (St. Louis, MO). Pluronic F127 ($PEO_{99}-PPO_{67}-PEO_{99}$, where PEO and PPO denote poly(ethylene oxide) and poly(propylene oxide), respectively) was provided by BASF Japan Ltd. (Osaka). 3-(4-(6-Phenyl)-1,3,5-hexatrienyl)phenylpropionic acid (DPHPA) was purchased from Molecular Probes (Eugene, OR). These materials were used without further purification. Other materials described later without notation were of the highest purity available.

Sample Preparation. Cubosome preparation has been described elsewhere.[22−24] Briefly, EPC and MO and F127 (8 wt % of total lipids, except for F127 concentration dependence experiments) were weighed and mixed in chloroform. After the solvent was evaporated, the mixture was dried in a vacuum. After they were roughly dispersed in Tris-buffer (10 mM Tris, 150 mM NaCl, pH 7.0) using a homogenizer (Microtec Co. Ltd., Chiba, Japan), further size reduction was performed using a high-pressure emulsifier (nanomizer system YSNM-1500-5, Yoshidakikai Co. Ltd., Nagoya) under a pressure of 35 MPa for 30 min at 40 °C. Total lipid concentration was ca. 10 mM.

For liposome preparation, buffer was added to the dry lipid mixtures that did not contain F127. The mixtures were vortexed and repeatedly freeze−thawed using liquid nitrogen and water, respectively. The dispersions were then extruded through a polycarbonate membrane with pore size of 100 nm (LiposoFast, Avestin Inc., Ottawa). Total lipid concentration was ca. 10 mM. The particle size of the dispersions was determined from dynamic light scattering measurements (Photal LPA-3000/3100; Otsuka Electronic Co., Osaka).

Nondispersed samples were also prepared. To the mixtures of lipids (ca. 0.15 mmol), an excess amount (1.5 mL) of buffer was added. The mixtures underwent a repeated freeze-and-thaw cycle and were kept at 4 °C for 1−2 weeks in an N_2 atmosphere before small-angle X-ray scattering (SAXS) experiments.

Small-Angle X-ray Scattering. The dispersions were concentrated (to ca. 300 mM of lipids) by ultrafiltration (Millipore) to obtain adequate intensity in SAXS experiments. These samples and the nondispersed samples were put into a glass capillary (W. Müller, Berlin, Germany; 1.5 mm o.d., 1/100 mm wall thickness). SAXS measurements were performed at 25 °C using a Kratky type camera (Rigaku Co., Tokyo) with Ni-filtered Cu Kα radiation (wavelength $\lambda = 1.54$ Å) generated by a Rigaku RU-200 rotating anode X-ray generator (50 kV, 200 mA). The slit-smeared diffraction patterns were detected by a position sensitive proportional counter, and desmeared by a standard procedure. For the dispersion, solvent scattering was subtracted. Scattering intensities were plotted against reciprocal spacing $s = 2(\sin\theta/2)/\lambda$, where θ is the scattering angle. Three hours or 30 min of exposure time was taken for the dispersed or nondispersed samples, respectively.

^{31}P NMR Spectroscopy. ^{31}P NMR measurements were performed at 25 °C on a Varian UNITY spectrometer at 121.5 MHz in the presence of a proton-decoupling field. The dispersions were put into an NMR tube (5 mm o.d.). D_2O was added to the dispersions in order to gain a lock and shim signal, and phospholipids concentration was ca. 20 mM. A paramagnetic-shifting reagent, praseodymium (III) nitrate (final concentration ~10 mM), was added, and the variance of the spectrum was traced. For measurements of the nondispersed systems, the samples were put into a glass capillary, and the capillary was placed into an NMR tube containing D_2O.

Fluorescence Measurements. For fluorescence experiments, 0.5 mol % of the fluorescence probe (DPHPA) was mixed with the lipid mixtures in the sample preparation described above. Fluorescence lifetime and anisotropy decay were measured by a time-correlated single-photon counting method on a HORIBA NAES-550 spectrofluorometer (Kyoto). The dispersions were put into a quartz cell (1 cm in width). For lifetime measurements of nondispersed (cubic phase) samples, the hydrated lipid mixtures were sandwiched between cover glass to measure foreground fluorescent light. The incident light from a hydrogen lamp with a full-width at half-maximum height of ca. 1.6 ns was passed through two sheets of HOYA U360 filters, and emission was detected through a HOYA L42 cutoff filter. For anisotropy measurements, the incident and emission light were passed through a polarizing prism and polarizing film, respectively. Measurements were performed at 25 or 37 °C.

The theory of the fluorescence experiments has been well described by Lakowicz.[26] The total fluorescence decay $I(t)$ is expressed by the summation of exponential decay functions with the fractional amplitude α_i and the fluorescence lifetime τ_i for the i-th component

$$I(t) = \sum \alpha_i \exp(-t/\tau_i) \tag{1}$$

The mean lifetime $\langle\tau\rangle$ was defined as

$$\langle\tau\rangle = \sum_{i=1}^{n} \alpha_i \tau_i^2 / \sum_{i=1}^{n} \alpha_i \tau_i \tag{2}$$

Experimentally obtained fluorescence decay $I^*(t)$ is a convolution of $I(t)$ and an intensity profile of pulsed excitation light $P(t)$

$$I^*(t) = \int_0^t P(t') I(t - t')\, \mathrm{d}t' \tag{3}$$

The values of τ_i were obtained by fitting the experimental fluorescence decay using eq 1 assuming double-exponential decay ($i = 1, 2$).

The fluorescence anisotropy $r(t)$ is expressed by the equation

$$r(t) = \frac{I_{\parallel}(t) - G I_{\perp}(t)}{I_{\parallel}(t) + 2G I_{\perp}(t)} \tag{4}$$

where $I_{\parallel}(t)$ and $I_{\perp}(t)$ are the parallel and perpendicular polarized components of the fluorescence after excitation by vertically polarized light, respectively, and G represents the compensating factor for the anisotropy sensitivity of the instrument, which is expressed as follows:

$$G = \int_0^{\infty} I_{HV}(t)\, \mathrm{d}t / \int_0^{\infty} I_{HH}(t)\, \mathrm{d}t \tag{5}$$

where $I_{HV}(t)$ and $I_{HH}(t)$ are the fluorescence intensities of the vertical and horizontal components after excitation by horizontally polarized light. In the wobble-in-cone model, DPHPA in lipid bilayers is assumed to wobble within a cone with a cone angle θ_C and with a wobbling diffusion coefficient D_W (see Figure 1), and thus $r(t)$ can be expressed as[27]

$$r(t) = (r_0 - r_\infty) \exp(-t/\phi) + r_\infty \tag{6}$$

where ϕ is the rotational correlation time, r_0 is the initial anisotropy at $t = 0$, and r_∞ is the residual anisotropy at infinite time. According to the method reported by Kawano et al.,[28] we measured DPHPA fluorescence anisotropy in glycerol at

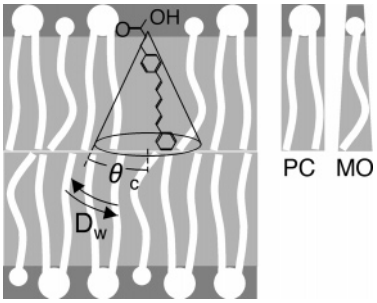

Figure 1. Schematic representation of the wobbling motion of DPHPA in lipid bilayers. θ_C and D_W represent the cone angle and the wobbling diffusion coefficient, respectively.

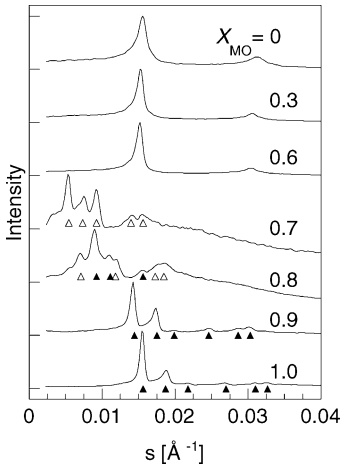

Figure 2. SAXS profiles of the nondispersed EPC/MO mixtures in Tris buffer. Open and closed triangles indicate the peak positions by which space groups of *Im*3*m* and *Pn*3*m* were identified, respectively.

−20 °C, where $r(t)$ remained practically at a constant value, and estimated that $r_0 = 0.390 \pm 0.003$. An apparent fluorescence anisotropy decay $r^*(t)$, which is obtained experimentally from eq 4, also convolutes the intensity profile of pulsed excitation light, however r_∞ can be directly figured out by averaging the values of $r^*(t)$ for a longer time region, where $r^*(t)$ remains at a constant value and the intensity profile of light source no longer affects the anisotropy decay. The order parameter S is given by the equation

$$S = (r_\infty/r_0)^{1/2} \tag{7}$$

S is related to the cone angle θ_C by $S = \cos\theta_C(1 + \cos\theta_C)/2$, and S increases when θ_C decreases. The value of ϕ is obtained by the fitting of $r^*(t)$ by eq 6 with deconvolution of the intensity profile of pulsed excitation light. The wobbling diffusion coefficients D_W can be expressed as[29]

$$D_W = \frac{1 - r_\infty/r_0}{6\phi} \tag{8}$$

Results

Phase Behavior of the Nondispersed Samples. The liquid crystalline samples of the mixtures were investigated by SAXS at 25 °C. Figure 2 shows SAXS profiles of the EPC/MO mixtures in excess buffer. Lamellar phase was observed at MO molar fractions (X_{MO}) up to 0.6, and the lamellar periodicity was almost independent of X_{MO} (64.1, 65.6, and 65.8 Å at $X_{MO} = 0$, 0.3, and 0.6, respectively). At X_{MO} more than 0.6, SAXS profiles corresponding to the bicontinuous cubic phases were obtained. This lamellar-cubic phase transition is attributed to the increased negative curvature by the addition of MO. At $X_{MO} = 0.7$, a space group of *Im*3*m*,[2] a typical diffraction for the bicontinuous cubic phase of the primitive type (C_P), with the lattice constant (a) of 266 Å was identified from five reflections [(110), (200), (211), (310), and (222)]. At $X_{MO} =$ 0.9 and 1.0, diffraction pattern of *Pn*3*m*[2] [(110), (111), (200), (211), (220), and (300) and/or (221)] was observed, suggesting a bicontinuous cubic phase of the diamond type (C_D). The lattice constant was 99.3 and 91.8 Å at $X_{MO} = 0.9$ and 1.0, respectively. Diffraction at $X_{MO} = 0.8$ was indicative of a coexistence of two cubic phases. Longer incubation of the sample at 25 °C (more than 1 week) did not change the diffraction pattern suggesting that the phases are equilibrated. Calculated diffraction profile[23] of the coexistence of C_D ($a = 158$ Å) and C_P ($a =$ 204 Å) reasonably reproduced the experimentally obtained diffraction (data not shown). The radius of narrow circular necks can be estimated by $a/2\sqrt{2}$ and $a/4$ for C_D and C_P, respectively, and are 66.6 ($X_{MO} = 0.7$), 55.7 and 50.9 ($X_{MO} = 0.8$), 35.1 ($X_{MO} = 0.9$), and 32.5 Å ($X_{MO} = 1.0$). The decrease in the radius of narrow circular necks suggests the increase in the negative curvature of the membrane with an increase in X_{MO}. The phase behavior was also investigated by ^{31}P NMR measurements as shown in Figure 3. An asymmetric peak indicative of the lamellar phase was observed at $X_{MO} = 0.6$. A sharp, symmetric peak at $X_{MO} = 0.7$ suggested that the lamellar phase was completely disappeared and an isotropic phase, and most probably the bicontinuous cubic phase, was formed. At $X_{MO} =$ 0.65, NMR spectrum provided both symmetric and asymmetric peaks, suggesting the coexistence of the lamellar and the cubic phases. A combination of SAXS and ^{31}P NMR revealed that the lamellar-cubic phase transition occurs at X_{MO} between 0.6 and 0.7.

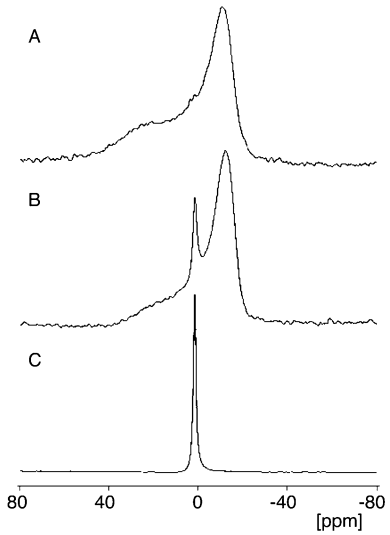

Figure 3. ^{31}P NMR spectra of the nondispersed EPC/MO mixtures in Tris buffer. $X_{MO} = 0.6$ (A), 0.65 (B), and 0.7 (C).

Formation of Liposomes and Cubosomes. The lamellar and cubic phases were dispersed in different ways. All the dispersions had a mean particle diameter of ca. 120 nm. For the EPC/MO lipid mixtures that formed the lamellar phase (X_{MO} up to 0.6), an extrusion method was applied to obtain liposomes. The liposome formation was confirmed by observing the peak splitting in ^{31}P NMR spectrum after the addition of Pr^{3+} ion (Figure 4). This observation is based on the fact that Pr^{3+} induces a lower magnetic field shift of the phosphorus signal of phospholipids located only in the outer leaflet of liposomes, because the ions can hardly pass through the liposome bilayer.

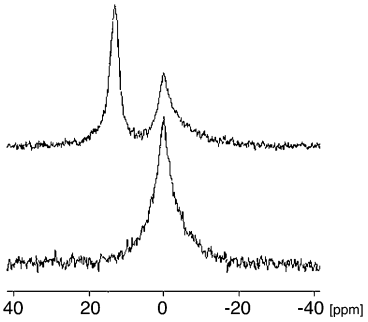

Figure 4. ^{31}P NMR spectra of the dispersions of the EPC/MO mixtures ($X_{MO} = 0.6$) with 8 wt % F127 before (lower) and after (upper) addition of Pr^{3+}.

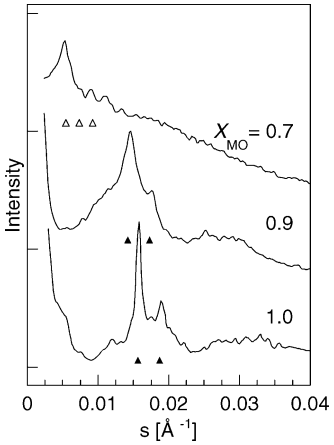

Figure 5. SAXS profiles of the dispersions of the EPC/MO mixtures with 8 wt % F127. Open and closed triangles indicate the first two or three peak positions of the corresponding nondispersed mixtures obtained in Figure 2.

For the mixtures containing higher fractions of MO, cubosomes were prepared by high-pressure emulsification with 8 wt % F127. The cubosome formation was verified by SAXS measurements as shown in Figure 5. The diffraction peaks were ambiguous compared with those from the nondispersed samples because the phases were fragmented into the submicron scale. Especially at higher EPC contents, increased lattice constant reduces the number of unit cell in a particle, making peaks weaker. At $X_{MO} = 1.0$, a peak at $s \sim 0.012$ Å indicates a presence of C_P phase in addition to C_D because nondispersed mixture of MO and F127 forms C_P phase.[22] A small peak at $s \sim 0.008$ Å at $X_{MO} = 0.9$ is also indicative of the presence of additional C_P phase. At $X_{MO} = 0.7$, some peaks which does not correspond to those of nondispersed mixture appeared. It is not clear at this time whether they are just a noise or an indication of another phase formation. However, in any case, the position of the maximum peak was the same with that of the corresponding nondispersed EPC/MO lipid mixtures, suggesting that the internal structure of these dispersed particles are almost identical to the nondispersed EPC/MO lipid mixtures. From these findings, it was concluded that liposomes ($X_{MO} = 0-0.6$) and cubosomes ($X_{MO} = 0.7-1.0$, with 8 wt % F127) could be prepared successfully.

Fluorescence Measurements for Cubosomes. If one aims to investigate the characteristics of cubic phases by fluorescence technique using cubosomes, the fluorescence probes should be located in the cubic phase of the particle interior, but not in the outer F127 layer. We performed fluorescence measurements to define the location of the fluorescence probe DPHPA in cubosome. First, fluorescence lifetime was measured in MO cubosomes with different F127 concentrations and compared

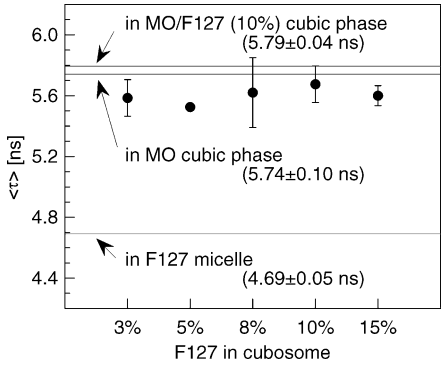

Figure 6. Mean fluorescence lifetimes ($\langle\tau\rangle$) of DPHPA in MO cubosomes with different F127 concentrations. Three solid lines denote the lifetime values in cubic phases and in F127 micelles as indicated in the figure. Each data represents the mean ± S. D. of three independent experiments.

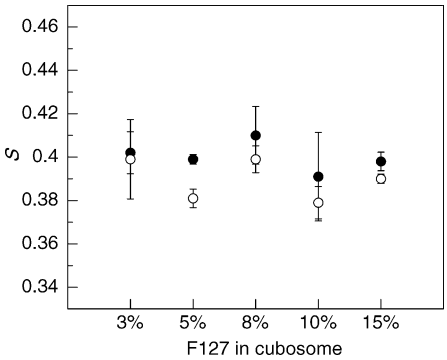

Figure 7. Order parameters (S) of DPHPA in MO cubosomes with different F127 concentrations obtained by time-resolved fluorescence anisotropy measurements at 25 °C (closed circles) and 37 °C (open circles). Each data represents the mean ± S. D. of three independent experiments.

with nondispersed MO cubic phase and F127 micelles. The results are shown in Figure 6. The mean lifetime $\langle\tau\rangle$ of DPHPA in cubosomes was independent of F127 concentration and was rather close to that of the nondispersed cubic phases formed by the MO or MO/F127 mixture than that of F127 micelles. Second, time-resolved fluorescence anisotropy measurements were performed for MO cubosome. The order parameter S of DPHPA in cubosomes did not depend on F127 concentration as shown in Figure 7. These independent experiments showed that the fluorescence probes are insensitive to F127 concentration suggesting that the probes are located not in the surface area but in the interior of cubosomes and that one can explore the lipid movement in the cubic phase using cubosomes.

Fluorescence Measurements for the EPC/MO Dispersions. We measured the time-resolved anisotropy of DPHPA in lamellar and cubic phases using liposomes and cubosomes, respectively. The order parameter of DPHPA was plotted as a function of X_{MO} in Figure 8. The order parameter S increased with an increase in X_{MO} for liposomes, suggesting the enhanced lateral pressure in the acyl chain region, that is, packing stress. On the other hand, S decreased when X_{MO} increased from 0.5 (liposome) to 0.7 (cubosome), which reflects the release of stress. The order parameter decreased further, when X_{MO} increased in cubosomes. At 37 °C, smaller order parameter values were detected than those at 25 °C because of higher lipid mobility, but a similar dependence on the MO fraction was observed.

Fluorescence Measurements for the POPC/MO Dispersions. We further explored this lipid composition dependence of the order parameter using POPC instead of EPC, to make

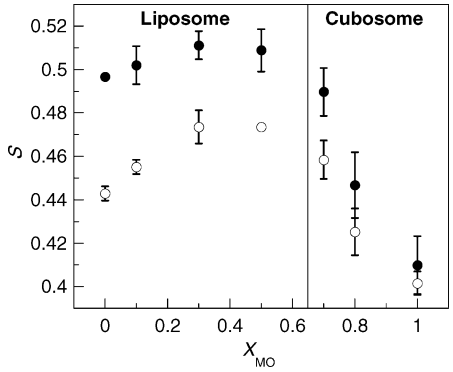

Figure 8. Order parameters (*S*) of DPHPA in EPC/MO liposomes ($X_{MO} \leq 0.5$) and cubosomes ($X_{MO} \geq 0.7$, with 8% F127) obtained by time-resolved fluorescence anisotropy measurements at 25 °C (closed circles) and 37 °C (open circles). Each data represents the mean ± S. D. of three independent experiments.

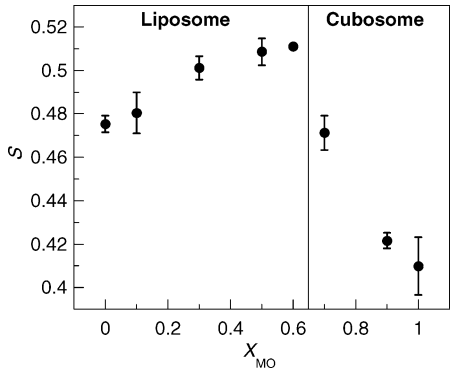

Figure 9. Order parameters (*S*) of DPHPA in POPC/MO liposomes ($X_{MO} \leq 0.6$) and cubosomes ($X_{MO} \geq 0.7$, with 8% F127) obtained by time-resolved fluorescence anisotropy measurements at 25 °C. Each data represents the mean ± S. D. of three independent experiments.

lipid composition more definitive. The result was shown in Figure 9. The composition dependence of the order parameter was more clearly observed than for EPC/MO dispersions. That is, *S* increased with the increase in X_{MO} for liposomes, decreased in the lamellar-cubic phase transition, and then further decreased with X_{MO} for cubosomes.

The wobbling diffusion coefficients D_W and the mean lifetime $\langle\tau\rangle$ were obtained by fitting the data of the time-resolved anisotropy and lifetime experiments, respectively. As shown in Figure 10, D_W and $\langle\tau\rangle$ were almost constant in liposomes, while $\langle\tau\rangle$ decreased and D_W increased with the increase in X_{MO} for cubosomes. We had anticipated that $\langle\tau\rangle$ values would be larger for cubosomes than liposomes because the cubic phases were considered more hydrophobic and preventive from penetration of water acting as a fluorescence quencher. However, the observed composition dependence of $\langle\tau\rangle$ was contrary to our expectation. A possible explanation of this behavior can be given as follows with reference to the corresponding change of D_W: The mobility of the fluorescence probes (D_W) in cubic phase increases after packing stress is released, which enhances the collision frequency of the probes with molecules working as fluorescence quenchers such as water and oxygen molecules, leading to the decrease in lifetime.

Discussion

Fluorescence measurements for nondispersed liquid crystalline samples are possible in principle, by measuring foreground fluorescent light as we did for the cubic phases of MO and MO/

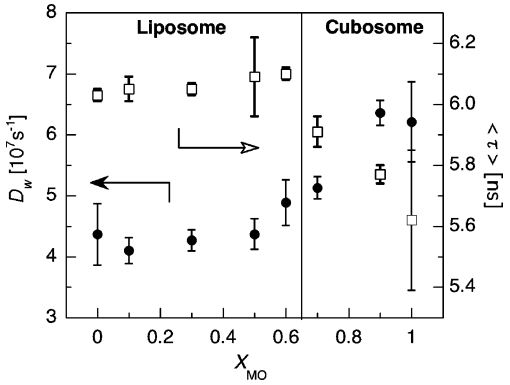

Figure 10. Wobbling diffusion coefficients (D_W, closed circles) and mean fluorescence lifetimes ($\langle\tau\rangle$, open squares) of DPHPA in POPC/MO liposomes ($X_{MO} \leq 0.6$) and cubosomes ($X_{MO} \geq 0.7$, with 8% F127) obtained by time-resolved fluorescence anisotropy measurements at 25 °C. Each data represents the mean ± S. D. of three independent experiments.

F127 mixture to obtain the lifetime. However, this method is not appropriate for the anisotropy measurements, since lipids and probes may orientate at a cell (quartz) surface, which influences the data. In this study, we attempted to measure fluorescence anisotropy of the bicontinuous cubic phase by dispersing it using an emulsifying agent, Pluronic F127.

For anisotropy measurement of the cubic phase using cubosomes, two prerequisite conditions should be satisfied, that is, 1) F127 must not influence the cubic structure, and 2) the fluorescence probe used must be located in the cubic phase. The former was proven by SAXS experiments. Although SAXS profiles of EPC/MO/F127 nondispersed mixtures showed that all the mixtures with X_{MO} between 0.7 and 1.0 form C_P phase in the presence of 8 wt % F127 (data not shown), the internal structure of dispersions at $X_{MO} = 0.9$ and 1.0 was C_D phase (Figure 5), which consists with the phase of nondispersed mixture without F127 (Figure 2). This suggests that in cubosome formation F127 molecules mostly absorb to the surface of the particles and few participate in the formation of the internal cubic structure.[22] The fluorescence lifetime (Figure 6) and anisotropy (Figure 7) values of DPHPA in MO cubosomes were independent of F127, by which the second requirement was approved. Thus, we demonstrated that cubosomes could be a powerful tool to figure out the properties of the cubic phases. In addition, the change in the anisotropy during the lamellar-cubic phase transition was first revealed by the combination with the dispersions of the lamellar phase, liposomes, as discussed below.

Using liposomes and cubosomes, the change in the order parameter of DPHPA was monitored in the lamellar-bicontinuous cubic phase transition as a nonlamellar-forming lipid (MO) was added to phospholipid bilayers. The order parameter for pure POPC liposomes was 0.475 ± 0.004, which is slightly smaller than that obtained when TMA-DPH was used (0.51−0.56) as a probe at 20 °C.[30] Considering that the order parameter decreases with temperature, our result (obtained at 25 °C) was reasonable. The order parameters are of course dependent upon the probes used,[31] yet their relative change with varied lipid compositions can be a measure of the change in lipid environments surrounding the probes. The order parameters of the palmitic acyl chain of POPC in bilayers at 27 °C determined by ^{2}H NMR were 0.15−0.43, depending on the position of the deuterated methylene position.[32]

Introduction of the nonlamellar-forming lipid to the bilayers makes them lose balance in headgroup size and acyl chain

volume and enhances lateral pressure in the acyl chain region, giving rise to packing stress. The increase in the order parameter in liposomes (Figures 8 and 9) indicates the generation of packing stress. This packing stress is considered to increase with the increase in the MO fraction and to be released by the transition to the cubic phase. Hence, a decrease in the order parameter by the transition from the lamellar ($X_{MO} = 0.6$) to the cubic phase ($X_{MO} = 0.7$) reflects the release of stress.

In nonlamellar phases, translational diffusion of the probes may influence the anisotropy data. Van der Meer et al. have developed a rotational diffusion model to investigate the orientation dynamics of the lipids in the H_{II} phase,[12−16,33,34] in which the rotational diffusion coefficient (D_H) and the wobbling diffusion coefficient (D_W) are within the same order (10^7 s^{-1}). In the simple wobble-in-cone model, which we applied in the present study, this lateral diffusion of the probes in the cubic phase is not taken into account, which might lead to an underestimate of the order parameters. However, we assume that the radius of curvature of the lipid layer in the cubic phase is so large that the effect of the lateral diffusion on anisotropy data can be ignored. This assumption is reasonable based on the following rough estimation for the MO cubic phase: D_H is given by $D_H = D_L/R^2$, where D_L is the lateral diffusion coefficient and R is the mean curvature of the surface at which the center of the emission dipole moment of the probes is located.[33] From the radius of narrow circular necks (32.5 Å) and assuming the distance from the bilayer center (minimal surface) to the neutral surface is 8.8 Å,[35] the mean curvature at the neutral surface is calculated to be $R = [\{1/(32.5 + 8.8) - 1/(32.5-8.8)\}/2]^{-1} = -111$ Å, where the negative figure represents negative curvature. The center of the emission dipole moment of DPHPA could be located around the neutral surface. Assuming the lateral diffusion coefficient (D_L) of the probe is identical to that of MO (16.9×10^{-12} m^2 s^{-1}),[36] D_H amounts to 1.37×10^5 s^{-1}, which is 2 orders of magnitude smaller than D_W (6.21×10^7 s^{-1}, see Figure 10). Cubic phases with larger cell unit sizes will provide smaller D_H values. Thus, it is concluded that the decrease in S on the lamellar-cubic phase transition reflects the release of stress.

The changes in S and D_W in the lamellar-cubic phase transition (Figures 8−10) were distinct from those in the lamellar-inverted hexagonal phase transition reported for phosphatidylcholine (PC)/phosphatidylethanolamine (PE) mixtures.[15,16] The transition of the PC/PE mixtures to H_{II} phase seems to occur at rather broad composition region. With the increase in PE% the order parameter starts to increase from the onset of a mesoscopic defect state (intermediate state of the transition) and stays high as the lipid mixtures finally reach the H_{II} phase. This indicates that packing stress remains high in the H_{II} phase. While D_W shows a maximum value in the intermediate state, it decreases and becomes constant in the inverted hexagonal phase. With support of FTIR data,[37,38] Cheng and co-workers[15,16] have concluded that the higher local orientation order and the more restricted wobbling motion in the H_{II} phase are attributed to the higher packing constraint imposed on the lipids near the glycerol backbone region. However, we suppose that the existence of an interstitial region[4] in the H_{II} phase is responsible for these distinct behaviors in both transitions. In the transition to the H_{II} phase, lipids achieve a negative mean curvature, but at the same time, their hydrocarbon chains are forced to stretch toward an extended conformation to fill the interstitial region. This constraint will make the hydrocarbon chains more ordered and restricted, and could be the reason the release of packing stress cannot be clearly observed. The bicontinuous cubic phases consist of a bilayer and are free from the interstitial region; consequently, lipids are released from packing stress by the lamellar-cubic phase transition. The results we obtained clearly demonstrate the release of packing stress.

In summary, the addition of MO ($X_{MO} = 0-0.6$) stores the PC flat bilayers with packing stress, which increases the acyl chain order. The flat bilayers transform their topology into curved ones to earn a negative mean curvature and to get rid of stress, resulting in a decrease in the order parameter ($X_{MO} = 0.6-0.7$). Further decrease in the order parameter in the cubic phase ($X_{MO} = 0.7-1.0$) could be due to the increased negative mean curvature, by which lipid molecules are allocated the more enhanced wedge-shaped regions.

Acknowledgment. This study was supported in part by a Grant-in-aid for Scientific Research from the Japanese Ministry of Education, Culture, Sports, Science and Technology (No. 15790026) and 21st Century COE Program "Knowledge Information Infrastructure for Genome Science". We gratefully acknowledge Dr. Hideki Matsuoka, Graduate School of Engineering, Kyoto University, for his support in SAXS measurements.

Supporting Information Available: SAXS profiles of the nondispersed EPC/MO/F127 mixtures showing formation of C_P phase. This material is available free of charge via the Internet at http://pubs.acs.org.

References and Notes

(1) Larsson, K. *J. Phys. Chem.* **1989**, *93*, 7304−7314.
(2) Lindblom, G.; Rilfors, L. *Biochim. Biophys. Acta* **1989**, *988*, 221−256.
(3) Seddon, J. M. *Biochim. Biophys. Acta* **1990**, *1031*, 1−69.
(4) Chernomordik, L. *Chem. Phys. Lipids* **1996**, *81*, 203−213.
(5) Bezrukov, S. M. *Curr. Opin. Colloid Interface Sci.* **2000**, *5*, 237−243.
(6) De Kruijff, B. *Nature* **1987**, *329*, 587−588.
(7) De Kruijff, B. *Curr. Opin. Chem. Biol.* **1997**, *1*, 564−569.
(8) Epand, R. M. *Biochim. Biophys. Acta* **1998**, *1376*, 353−368.
(9) Sen, A.; Isac, T. V.; Hui, S. W. *Biochemistry* **1991**, *30*, 4516−4521.
(10) Ruiz-Argüello, M. B.; Goñi, F. M.; Alonso, A. *Biochemistry* **1998**, *37*, 11621−11628.
(11) Attard, G. S.; Templer, R. H.; Smith, W. S.; Hunt, A. N.; Jackowski, S. *Proc. Natl. Acad. Sci. U.S.A.* **2000**, *97*, 9032−9036.
(12) Cheng, K. H. *Biophys. J.* **1989**, *55*, 1025−1031.
(13) Cheng, K. H. *Chem. Phys. Lipids* **1990**, *53*, 191−202.
(14) Chen, S.-Y.; Cheng, K. H. *Chem. Phys. Lipids* **1990**, *56*, 149−158.
(15) Chen, S.-Y.; Cheng, K. H. *Biophys. J.* **1996**, *71*, 878−884.
(16) Chen, S.-Y.; Cheng, K. H.; van der Meer, B. W. *Biochemistry* **1992**, *31*, 3759−3768.
(17) Cheng, K. H.; Chen, S.-Y.; Butko, P.; van der Meer, B. W.; Somerharju, P. *Biophys. Chem.* **1991**, *39*, 137−144.
(18) Cheng, K. H.; Somerharju, P.; Sugar, I. *Chem. Phys. Lipids* **1994**, *74*, 49−64.
(19) Butko, P.; Cheng, K. H. *Chem. Phys. Lipids* **1992**, *62*, 39−43.
(20) Victorov, A. V.; Taraschi, T. F.; Hoek, J. B. *Biochim. Biophys. Acta* **1996**, *1283*, 151−162.
(21) Gawrisch, K.; Holte, L. L. *Chem. Phys. Lipids* **1996**, *81*, 105−116.
(22) Nakano, M.; Sugita, A.; Matsuoka, H.; Handa, T. *Langmuir* **2001**, *17*, 3917−3922.
(23) Nakano, M.; Teshigawara, T.; Sugita, A.; Leesajakul, W.; Taniguchi, A.; Kamo, T.; Matsuoka, H.; Handa, T. *Langmuir* **2002**, *18*, 9283−9288.
(24) Kamo, T.; Nakano, M.; Leesajakul, W.; Sugita, A.; Matsuoka, H.; Handa, T. *Langmuir* **2003**, *19*, 9191−9195.
(25) Monduzzi, M.; Ljusberg-Wahren, H.; Larsson, K. *Langmuir* **2000**, *16*, 7355−7358.
(26) Lakowicz, J. R. *Principles of fluorescence spectroscopy*, 2nd ed.; Kluwer Academic/Plenum Publishers: New York, 1999.

(27) Lipari, G.; Szabo, A. *Biophys. J.* **1980**, *30*, 489−506.
(28) Kawano, S.; Kinoshita, K., Jr.; Ikegami, A. *Biochemistry* **1977**, *16*, 2319−2324.
(29) van der Meer, B. W.; Pottel, H.; Herreman, W.; Ameloot, M.; Hendrickx, H.; Schroder, H. *Biophys. J.* **1984**, *46*, 515−523.
(30) van Langen, H.; Levine, Y. K.; Ameloot, M.; Pottel, H. *Chem. Phys. Lipids* **1987**, *140*, 394−400.
(31) Pap, E. H. W.; ter Horst, J. J.; van Hoek, A.; Visser, A. J. W. G. *Biophys. Chem.* **1994**, *48*, 337−351.
(32) Seelig, A.; Seelig, J. *Biochemistry* **1977**, *16*, 45−50.
(33) van der Meer, B. W.; Cheng, K. H.; Chen, S.-Y. *Biophys. J.* **1990**, *58*, 1517−1526.
(34) Chen, S.-Y.; Cheng, K. H.; van der Meer, B. W.; Beechem, J. M. *Biophys. J.* **1990**, *58*, 1527−1537.
(35) Chung, H.; Caffrey, M. *Biophys. J.* **1994**, *66*, 377−381.
(36) Eriksson, P.-O.; Lindblom, G. *Biophys. J.* **1993**, *64*, 129−136.
(37) Cheng, K. H. *Chem. Phys. Lipids* **1991**, *60*, 119−125.
(38) Cheng, K. H. *Chem. Phys. Lipids* **1994**, *70*, 43−51.